HOKKAIDO UNIVERSITY

Title	Development of a Nonlinear Mechanical Model for Fiber Concrete-Enhanced Steel (FCES) Columns with Flexural-shear Failure Mode
Author(s)	Chiu, Chien-Kuo; Ghifari, Fikri
Relation	Proceedings of the 10th International Symposium on Reliability Engineering and Risk Management (ISRERM 2026), June 28 - July 1, 2026, Sapporo, Japan
Citation	Proceedings of the 10th International Symposium on Reliability Engineering and Risk Management (ISRERM 2026)
Issue Date	2026-07-01
Doc URL	https://hdl.handle.net/2115/100465
Type	conference paper
File Information	C000186_1.pdf



Hokkaido University Collection of Scholarly and Academic Papers : HUSCAP

10th International Symposium on Reliability Engineering and Risk Management (ISRERM 2026),
28 June-01 July 2026, Sapporo, Japan
Kitahara, T., Miyamori, Y. & Beer, M. (editors)

Development of a Nonlinear Mechanical Model for Fiber Concrete-Enhanced Steel (FCES) Columns with Flexural-shear Failure Mode

Chien-Kuo Chiu[1], and Fikri Ghifari[2]*

[1]*Department of Civil and Construction Engineering, National Taiwan University of Science and Technology, Taipei, Taiwan.*
E-mail: ckchiu@mail.ntust.edu.tw
[2]*Department of Civil and Construction Engineering, National Taiwan University of Science and Technology, Taipei, Taiwan.*
E-mail: D11105821@mail.ntust.edu.tw
**Corresponding Author*

The Fiber Concrete-Enhanced Steel (FCES) column is a composite column consisting only of a steel section and fiber-reinforced concrete, without conventional reinforcement, thereby reducing construction complexity. Currently, ASCE 41 does not provide modeling parameters for FCES columns. In addition, the AIJ guidelines propose a mechanical model for FCES columns based on the assumption of a flexural failure mode. However, this model does not reflect the actual behavior observed in many experimentally tested FCES columns reported in previous studies, where the predominant failure mode is flexural-shear. The proposed model is modified from an existing Steel-Reinforced Concrete (SRC) model and is validated using 25 FCES column experimental datasets. The model is applicable to concrete compressive strengths ranging from 31.2 MPa to 65.3 MPa, Axial load ratios of 0.09-0.3, Fiber contents of 1-2%, XH-steel ratios of 5.64–6.65%, and H-steel ratios of 3–7.01%. The considered fiber types include Hybrid fiber concrete (HyFC), Steel fiber concrete (SFC), and PVA fiber concrete (PVA-FC). The proposed model defines four key points—cracking, peak, stable post-peak, and ultimate—based on elastic analysis, P–M interaction, and modified deformation relationships. The results demonstrate conservative predictive performance.

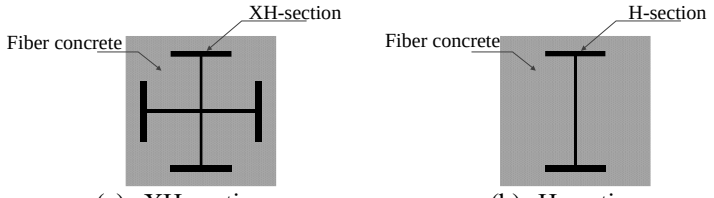
Keywords: Fiber concrete-enhanced steel (FCES), nonlinear mechanical model, fiber concrete, flexural-shear failure mode

1 Introduction

The Steel-Reinforced Concrete (SRC) column is a composite system of a steel section and reinforced concrete, providing improved seismic capacity through their combined resistance (Gautham & Sahoo, 2021). However, the conventional reinforcement can create construction difficulties. Therefore, recent studies propose the Fiber Concrete-Enhanced Steel (FCES) column, consisting of a steel section and fiber concrete following AIJ guidelines (AIJ 2022, 2022). By eliminating conventional reinforcement, the steel section can be enlarged while maintaining strength comparable to SRC columns and the fibers effectively limit cracking even under large deformations.

The development of mechanical models suitable for nonlinear seismic analysis remains limited. For practical seismic evaluation, pushover analysis requires a reliable lateral force-deformation relationship. ASCE 41(ASCE, 2017) provides procedures for predicting lateral force–deformation relationships; however, it does not include modeling parameters for FCES columns. Although the AIJ guidelines (AIJ 2022, 2022) propose a mechanical model for FCES columns, this model is developed under the assumption of a flexural failure mode. This assumption is inconsistent with experimental observations reported in previous studies, which indicate that FCES columns predominantly exhibit flexural–shear failure (Chiu et al., 2025; Fujimoto et al., 2009; Kuramoto, 2008; Shi et al., 2011).

Accordingly, the objective of this study is to develop a mechanical model for FCES columns incorporating various types of fiber concrete, with the model formulated for columns governed by flexural-shear failure mode. Previous studies (Chiu et al., 2025; Fujimoto et al., 2009; Kuramoto, 2008) have shown that FCES and SRC columns exhibit similar mechanical behavior, particulary in terms of their backbone curves. This similarity suggests that established SRC-based mechanical model can serve as a foundation for developing an FCES mechanical model. The mechanical model is validated using 25 FCES column tests summarized in Table 1. Two steel section types are used, as illustrated in Figure 1.



(a) XH-section (b) H-section

Figure 1. Types of steel section

Table 1. Properties of tested columns

Ref	b_c	h_c	f'_{ca}	n	Steel section	f_{ya}	V_f

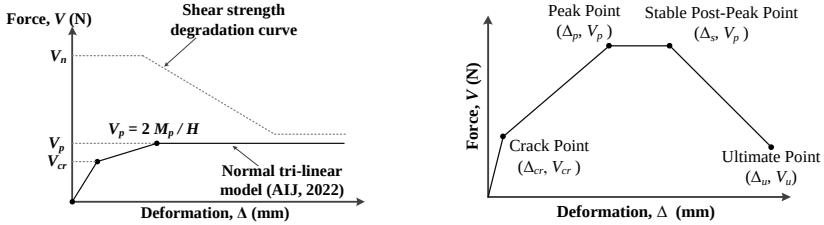
	Specimen ID	(mm)	(mm)	(MPa)			(MPa)	Fiber type	(%)
(Chiu et al., 2025)	HFCES	400	400	33.2	0.25	XH 300 x 150 x 6.5 x 9	373	AR-GF & PPF	2
(Fujimoto et al., 2009)	VF1-CES	400	400	52.3	0.11	XH 300 x 150 x 6.5 x 9	337	PVA	1
	VF2-CES	400	400	55.5	0.11	XH 300 x 150 x 6.5 x 9	337	PVA	2
	SF2-CES	400	400	65.3	0.09	XH 300 x 150 x 6.5 x 9	337	Steel	2
	VF2N3	330	330	46	0.22	XH 250 x 125 x 6 x 9	393	PVA	2
	VF2N5	330	330	46	0.4	XH 250 x 125 x 6 x 9	393	PVA	2
(Adachi et al., 2002)	SF2	400	400	65.3	0.09	XH 300 x 150 x 6.5 x 9	336.8	Steel	2
	VF1	400	400	52.3	0.11	XH 300 x 150 x 6.5 x 9	336.8	PVA	1
	VF2	400	400	55.5	0.11	XH 300 x 150 x 6.5 x 9	336.8	PVA	2
(Shi et al., 2011)	B30b	300	300	43.01	0.3	H 200 x 150 x 6 x 9	354	PVA	1
	B30c	300	300	45.09	0.3	H 200 x 150 x 6 x 9	354	PVA	1
	B25b	300	300	46.21	0.25	H 200 x 150 x 6 x 9	354	PVA	1
	B25c	300	300	45.11	0.25	H 200 x 150 x 6 x 9	354	PVA	1
	A2	300	300	43.9	0.18	H 200 x 150 x 6 x 9	277.7	PVA	1
	B1	300	300	43.2	0.09	H 200 x 150 x 6 x 9	277.7	PVA	1
	B2	300	300	43.9	0.18	H 200 x 150 x 6 x 9	277.7	PVA	1
	B3H	300	300	45	0.3	H 200 x 150 x 6 x 9	277.7	PVA	1
	B3-F	300	300	33.6	0.28	H 200 x 150 x 6 x 9	282.3	PVA	1.5
	B3MB	300	300	36.4	0.28	H 200 x 180 x 8 x 12	287.1	PVA	1
	B3MB-F	300	300	34.7	0.28	H 200 x 180 x 8 x 12	287.1	PVA	1.5
(Hiroyuki et al., 2000)	SF	400	400	31.2	0.2	XH 300 x 150 x 6.5 x 9	322.6	PVA	1.5
	SF-b	400	400	34.8	0.2	XH 300 x 150 x 6.5 x 9	322.6	PVA	1.5
(Kawamoto et al., 2008)	FRC CES	200	300	52.9	0.1	H 200 x 100x 3.2 x 6	318	PVA	1.5
	PCa CES1	200	300	51.6	0.1	H 200 x 100x 3.2 x 6	318	PVA	1.5
	PCa CES2	200	300	44.3	0.1	H 200 x 100x 3.2 x 6	318	PVA	1.5

Notes:

- b_c = Width of the section
- h_c = Height of the section
- f'_{ca} = Actual compressive strength of the concrete
- n = Applied axial compression load ratio
- f_{ya} = Actual yield strength of the steel
- V_f = Fiber ratio

2 Proposed Mechanical Model of an FCES Column

For building structural analysis, a nonlinear mechanical model is needed to describe force–deformation behavior. The AIJ Guidelines (AIJ 2022, 2022) provide a normal tri-linear model (Figure 2a) assuming flexural failure. However, studies show that strength remains stable up to a point before shear deformation causes degradation (Fujimoto et al., 2009; Kawamoto et al., 2008; Kuramoto, 2008). This study proposes a more reliable method, constructing the FCES force–deformation relationship similarly to the SRC model by Shang et al. (Shang et al., 2023) (Figure 2b). The backbone curve here connects four critical points: crack, peak, stable post-peak, and ultimate.



(a) AIJ mechanical model(AIJ 2022, 2022) (b) Proposed mechanical model

Figure 2. Mechanical model of an FCES column.

2.1 *Crack Point*

Based on reference (Shang et al., 2023), the lateral force corresponding to the crack point can be calculated using an elastic analysis formula, as follows:

$$\boldsymbol{V_{cr}} = \frac{\boldsymbol{4\left(f_r + {}^{N}/_{A_g}\right) I_g}}{\boldsymbol{Lh}} \tag{1}$$

where $\boldsymbol{V_{cr}}$ is the crack strength of the column (N); $\boldsymbol{f_r}$ is the fiber concrete flexural strength (MPa); $\boldsymbol{N}$ is the applied axial load (N); $\boldsymbol{A_g}$ is the gross section area (mm^2); $\boldsymbol{I_g}$ is the total moment of inertia (mm^4); $\boldsymbol{L}$ is the length of the column (mm) and $\boldsymbol{h}$ is the depth of the cross-section (mm).

The lateral deformation corresponding to the crack point can be assumed to be the sum of flexural, shear, and bar-slip deformations, according to reference (Shang et al., 2023). Hooke's law is used to calculate the column's deformation. Additionally, since an FCES column does not have rebars for resisting bending moments, the bar-slip deformation is neglected:

$$\Delta_{cr} = \Delta_{cr,f} + \Delta_{cr,sh} \tag{2}$$

$$\Delta_{cr,f} = \frac{V_{cr}L^3}{12(E_{cf}I_c + E_sI_s)} \tag{3}$$

$$\Delta_{cr,sh} = \frac{V_{cr}L}{3(G_{cf}A_{cf} + G_sA_w)} \tag{4}$$

where Δ_{cr} is the column deformation at the crack point (mm); $\Delta_{cr,f}$ and $\Delta_{cr,sh}$ are the flexural and shear deformations at crack point (mm); E_{cf} and E_s are the elastic modulus of fiber concrete and steel, respectively (MPa); I_{cf} and I_s are the moments of inertia of fiber concrete and steel, respectively (mm^4); G_{cf} and G_s are the shear modulus of fiber concrete and steel (MPa), respectively (MPa); A_{cf} and A_{sw} is the cross-sectional area of fiber concrete and the steel web (mm^2).

2.2 *Peak Point*

The lateral force corresponding to the peak point can be calculated based on the AISC P-M interaction curve (American Institute of Steel Construction, 2022) for a given axial load. Additionally, the concrete compressive strength confined by the steel section is considered. The lateral force corresponding to the peak point is calculated as follows:

$$V_p = \frac{2M_p}{L} \tag{5}$$

where V_p is the lateral force corresponding to the maximum moment strength of the column (N) and M_p is the maximum moment strength under a given axial load (N-mm). The definition of confined and unconfined concrete is shown in Figure 3. The confinement effect is modified from Wang et al. (J. Wang et al., 2023) due to the absence of rebars, as shown below:
For highly confined areas, H1:

$$f_{le,H1} = \frac{A_e}{A_g}\left(\frac{f_{u,w}t_w}{b - t_w}\right) \tag{6}$$

For partially confined areas, H2:

$$f_{le,H2} = f_{le,H1}\left(\frac{(b - t_w)}{h - t_w - 2t_f}\right) \tag{7}$$

where A_e is the total area confined by the steel (mm^2), $f_{u,w}$ is the ultimate strength of the web (MPa), t_w is the web thickness (mm), t_f is the flange thickness (mm), b is the width of the column cross-section (mm), and h is the height of the column cross-section (mm).



(a) Confined concrete area by steel section (b) Unconfined concrete area

Figure 3. Concrete confinement

The compressive strength provided by the confined steel area can be calculated according to Shang et al. (Shang et al., 2023) as shown:

$$f_{ccf} = \left(-1.254 + 2.254\sqrt{1 + \frac{7.94f_{le}}{f'_{cf}}} - 2\frac{f_{le}}{f'_{cf}}\right)f'_{cf} \tag{8}$$

where f_{ccf} is the confined fiber concrete strength (MPa), and f_{le} is the effective confining pressure based on Eqs (6)-(7). To account for the confinement effect and combine all compressive strengths, a weighted average is used, as the confined strength values are derived from three different elements (Shang et al., 2023). The modified confined hybrid-fiber concrete compressive strength is then given by:

$$f'_{ccf} = \frac{f'_{cf}A_{ucf} + f'_{ccf,p}A_{cc,H2} + f'_{ccf,h}A_{cc,H1}}{A_{cf}} \quad (9)$$

where A_{ucf}, $A_{cc,H2}$, $A_{cc,H1}$, and A_{cf} are the cross-sectional area of unconfined, partially confined, highly confined, and total fiber concrete (mm^2).

The deformation corresponding to the peak point is defined based on the secant stiffness of the column (Shang et al., 2023; B. Wang et al., 2019). According to the reference (B. Wang et al., 2019), the peak deformation is calculated using Eq. (10). Additionally, the secant stiffness of the column K_s is determined based on the reduction of elastic stiffness. The reduction factor is observed based on the previous studies (Shi et al., 2011; Son Vu & Li, 2024). It is observed that even small changes in axial load ratio significantly influence the deformation capacity of FCES columns. Therefore, the secant stiffness is calculated as shown in Eq. (11) for XH section and Eq. (12) for H section.

$$\Delta_p = \frac{V_p}{K_s} \quad (10)$$

$$K_s(\text{XH section}) = (0.898n + 0.2)K_e \quad (11)$$

$$K_s(\text{H section}) = (1.83n + 0.01)K_e \quad (12)$$

2.3 *Stable Post-Peak Point*

Before the strength drops significantly, peak strength can be maintained due to ductility (Shang et al., 2023). Therefore, the deformation at this stage for FCES columns is adapted from reference (Shang et al., 2023), with the transverse reinforcement effect removed since FCES columns contain no transverse reinforcement:

$$\Delta_s = \Delta_p + 0.5L\left(0.042 - 0.043n - 0.023\frac{V_p}{V_{col}}\right) \quad (13)$$

where Δ_s is the stable post-peak deformation (mm) and V_{col} is the shear strength of the column (N).

2.4 *Ultimate Point*

The ultimate strength includes contributions from both the concrete and the steel section. The steel section provides stable enhanced resistance due to confinement effect, but the strength of non-crushed concrete is difficult to estimate accurately. Thus, ASCE 41 recommends applying a reduction factor to account for its contribution. The selected formula, adapted from the reference (Shang et al., 2023), is detailed as follows:

$$V_u = (0.24 - 0.4n)V_p + \frac{f_y Z_x}{0.5L} \quad (14)$$

where V_u is the lateral ultimate force (N); f_y is the yield strength of the steel section (MPa) and Z_x is the plastic modulus of the steel section (mm^3).

The ultimate deformation is calculated as the sum of Δ_p and the product of the ultimate plastic angle and the length, as shown in Eq. (15) (Shang et al., 2023). Experimental evidence reported (Shi et al., 2011; J. Wang et al., 2023) indicates that the encased steel section ratio (ρ) provides effective confinement and stable load sharing, leading to enhanced deformation capacity at the ultimate state. Therefore, the steel section ratio is explicitly incorporated into the proposed model to represent confinement effects, as shown in Eq. (16) for XH section and Eq. (17) for H section.

$$\Delta_u = \Delta_p + 0.5L\theta_u \quad (15)$$

$$\theta_u(\text{XH section}) = 0.0026\rho + 0.012 \quad (16)$$

$$\theta_u(\text{H section}) = 0.0043\rho + 0.0035 \quad (17)$$

3 Model Verification using the Existing Experimental Data

The model is validated with 25 columns experimental datasets, as presented in Table 1. The proposed model is applicable to FCES columns with concrete compressive strengths ranging from 31.2 Mpa to 65.3 Mpa, axial load ratios from 0.09 to 0.40, and fiber contents between 1.0% and 2.0%. The considered fiber types include hybrid fiber cocnrete (HyFC), steel fiber concrete (SFC), and PVA fiber concrete (PVA-FC). The steel section ratio ranges from 5.64% to 6.65% for XH sections and from 3.0% to 7.01% for H sections. The corresponding ratio between calculated and tested results is presented in Table 2.

Table 2. Ratio of the calculated to tested results

Ref.	Specimen ID	Crack		Peak		Ultimate	
		DR_C/DR_T	V_C/V_T	DR_C/DR_T	V_C/V_T	DR_C/DR_T	V_C/V_T
(Chiu et al., 2025)	HFCES	0.794	0.999	0.687	0.885	0.903	0.715
(Fujimoto et al., 2009)	VF1-CES	0.621	0.774	0.935	0.967	1.006	0.660
	VF2-CES	0.779	0.908	0.912	0.940	1.006	0.568
	SF2-CES	0.706	0.910	0.610	0.979	0.936	0.633
	VF2N3	0.747	0.860	0.454	0.980	0.933	0.521
	VF2N5	1.002	0.854	0.754	0.994	0.973	0.536

(Adachi et al., 2002)	SF2	0.649	0.953	0.634	0.981	0.855	0.673
	VF1	0.757	0.828	0.920	0.987	0.900	0.744
	VF2	0.635	0.812	0.855	0.999	0.984	0.647
(Shi et al., 2011)	B30b	0.853	0.656	0.886	0.893	1.006	0.952
	B30c	0.802	0.655	0.974	0.993	1.039	0.937
	B25b	0.817	0.706	0.859	0.973	0.802	0.786
	B25c	0.893	0.552	0.864	0.960	0.817	0.867
	A2	0.570	0.650	0.848	0.959	0.856	0.662
	B1	0.738	0.565	0.518	0.984	0.764	0.683
	B2	0.971	0.650	0.684	0.956	0.793	0.673
	B3H	0.704	0.702	1.091	0.902	1.079	0.890
	B3-F	0.779	0.685	0.896	0.970	0.852	0.904
	B3MB	0.906	0.793	1.043	0.958	1.034	1.027
	B3MB-F	0.874	0.809	1.119	0.918	1.025	1.043
(Hiroyuki et al., 2000)	SF	0.949	0.999	0.330	0.965	0.999	0.637
	SF-b	0.899	0.997	0.541	0.990	0.907	0.639
(Kawamoto et al., 2008)	FRC CES	0.582	0.922	0.501	0.940	0.572	0.919
	PCa CES1	0.588	0.919	0.462	0.987	0.547	0.828
	PCa CES2	0.623	0.899	0.582	0.984	0.558	1.009
Mean		0.770	0.802	0.758	0.962	0.886	0.766
CoV		0.166	0.170	0.287	0.034	0.169	0.208

Notes:

- DR_C/DR_T = ratio of calculated and tested drift
- V_C/V_T = ratio of calculated and tested force

For the crack point, the average ratio between the calculated and experimental results is less than 1.0, indicating that the proposed equation predicts the crack strength and deformation conservatively, as shown in Table 2. For peak point verification, the calculated peak strength closely matches the experimental values, suggesting that the modified confinement effect proposed by Wang et al. (J. Wang et al., 2023), which accounts for the absence of rebar, is highly effective. The coefficient of variation (COV) of the calculated peak strength, as listed in Table 2, is 0.03, demonstrating that the AISC P–M interaction curve, incorporating the modified compressive strength of confined fiber-reinforced concrete, yields reliable peak strength predictions.

The proposed reduction factor to calculate the secant stiffness can be effectively used to conservatively estimate the peak deformation, showing good agreement with the experimental results, except for the specimens from the reference (Shi et al., 2011). Specimens B3H, B3MB, and B3MB-F had wider steel flanges (Shi et al., 2011), and it is observed that using a wider steel flange could initiate shear cracks extending from the column head at a drift ratio of approximately 1%, making it difficult to develop peak deformation. Further research is required to investigate the effects of higher axial loading ratios on column performance, as the available experimental data are limited to a maximum axial loading ratio of 0.4.

At the ultimate point, the strength calculated using the method proposed by the previous studies (Shang et al., 2023) conservatively predicts the ultimate strength, with an average ratio of 0.76, indicating the failure mode aligns reasonably well with the results. For B3MB and B3MB-F, a wider steel flange can initiate shear cracks extending from the column head at a drift ratio of approximately 1%. These cracks then widened significantly along the flange surface as the concrete cover became thinner, resulting in rapid strength degradation (Shi et al., 2011).

For ultimate deformation, the proposed formula conservatively predicts the deformation capacity, with an average ratio of 0.886 and a COV of 0.15—excluding the specimens reported in reference (Shi et al., 2011). For specimen B3H, the ultimate deformation was not well developed. According to reference (Shi et al., 2011), high axial strain occurred before reaching the ultimate point, which may explain the limited development of ultimate deformation. Restated, further research is required to investigate a higher steel section ratio on the ultimate deformation, as the available experimental data are limited.

4 Conclusions

This study proposed a nonlinear mechanical model for FCES columns with flexural-shear failure mode, removing the reinforcement effect, and incorporating various types of fiber. The model defined four critical points—lateral crack, peak, stable post-peak, and ultimate—allowing straightforward application using ASCE 41-based parameters and without reinforcement data. Validation against 25 experimental datasets showed that the model conservatively predicts strength and deformation within the tested ranges of concrete strength (31.2–65.3 MPa), axial load ratio (0.09–0.30), various fiber types (HyFC, SFC, PVA-FC), fiber content (1–2 %), XH-steel section ratios (5.64–6.65 %), and H-Steel section ratios (3–7.01%). Overall, the proposed model provides a practical and

mechanics-based tool for seismic performance assessment of FCES columns. Further research is required to investigate the influence of higher axial load ratios and larger steel section ratios on the proposed mechanical model.

References

Adachi, T., Kuramoto, H., & Kawasaki, K. (2002). Steel Concrete Composite Structural Columns Using Fiber Reinforced Concrete: Experimental study on structural performance (in Japanese). *Concrete Engineering Annual Proceedings*, *24*.

AIJ 2022. (2022). *AIJ Guidelines for Structural Design of Concrete Encased Steel (CES) Buildings Based on Performance Evaluation Concept (In Japanese)*. Architectural Institute of Japan.

American Institute of Steel Construction. (2022). *Specification for Structural Steel Buildings*. https://www.aisc.org/

ASCE. (2017). *ASCE/SEI, 41-17 : seismic evaluation and retrofit of existing buildings*. American Society of Civil Engineers.

Chiu, C.-K., Ghifari, F., Chi, T.-L., & Liao, I.-H. (2025). Experimental investigation on seismic capacity of concrete-enhanced steel columns using hybrid-fiber concrete with alkali-resistant-glass fiber and polypropylene fiber. *Structure and Infrastructure Engineering*, 1–17. https://doi.org/10.1080/15732479.2025.2494128

Fujimoto, T., Kuramoto, H., & Matsui, T. (2009). CES columns with built-in intersecting H-section steel frames: Structural performance (in Japanese). In *The 8th Symposium on Utilization of Composite/Synthetic Structures*.

Gautham, A., & Sahoo, D. R. (2021). Behavior of steel-reinforced composite concrete columns under combined axial and lateral cyclic loading. *Journal of Building Engineering*, *39*. https://doi.org/10.1016/j.jobe.2021.102305

Hiroyuki, T., Kurosaki, M., & Kuramoto, H. (2000). Steel Concrete Structural Column Using High Toughness Cement Material: Experimental Study on Restoring Force Characteristics (in Japanese). *Concrete 11th Grade Papers*, *22*.

Kawamoto, T., Kuramoto, H., Matsui, T., Fujimoto, T., & Osaki, J. (2008). BEHAVIOR OF PRECAST CES COLUMNS FOR MIDDLE AND LOW-RISE HOUSES. *The 14th World Conference on Earthquake Engineering*.

Kuramoto, H. (2008). Behavior of Columns in Composite CES Structural System. *International Conference on Composite Construction in Steel and Concrete*. https://doi.org/https://doi.org/10.1061/41142(396)37

Shang, C., Xue, Y., Yang, Y., Yu, Y., & Yu, J. (2023). Lateral load-displacement response of flexure-dominant concrete-encased steel columns based on ASCE/SEI 41. *Journal of Constructional Steel Research*, *203*. https://doi.org/10.1016/j.jcsr.2023.107845

Shi, J., Jose CASTRO, J., Matsui, T., & Kuramoto, H. (2011). Structural Experiment and Evaluation of Deformability of CES Column with H-Shaped Steel Frame (In Japanese). *Proceedings of the Japan Concrete Institute*, *33*.

Son Vu, N., & Li, B. (2024). Seismic performance of flexural reinforced concrete columns subjected to varying axial forces. *Engineering Structures*, *310*. https://doi.org/10.1016/j.engstruct.2024.118090

Wang, B., Huo, G., Sun, Y., & Zheng, S. (2019). Hysteretic behavior of steel reinforced concrete columns based on damage analysis. *Applied Sciences (Switzerland)*, *9*(4). https://doi.org/10.3390/app9040687

Wang, J., Cui, M., Jiao, Y., & Fang, X. (2023). Axial stress-strain characteristics and confinement mechanism of concrete-encased steel composite columns: An analytical model. *Journal of Building Engineering*, *72*. https://doi.org/10.1016/j.jobe.2023.106656